

The Impacts of Assimilating Fengyun-4A Atmospheric Motion Vectors on Typhoon Forecasts

Keyi Chen¹ and Peigen Guan²

¹Chengdu University of Information Technology

²Chengdu University of Information&Technology

January 3, 2023

Abstract

Atmospheric motion vectors (AMVs), known as cloud track winds, have positive impacts on global numerical weather forecasts (NWP). In this study, AMVs retrieved from Fengyun-2G and Fengyun-4A are compared in their data quality and impacts on the typhoon forecasts in order to investigate the differences between the first and second generation of the geostationary meteorological satellites of China. This report conducted data evaluation and assimilation-forecasting experiments on FY-2G and FY-4A atmospheric motion vector (AMVs), respectively. The results show that the AMVs data of FY-4A are of better quality than those of FY-2G and assimilating the AMVs of FY-2G and FY-4A have a neutral to slightly positive impacts on typhoon forecasts, which is quite encouraging for the operational use in the future.

Hosted file

951425_0_art_file_10506316_rmf51q.docx available at <https://authorea.com/users/563402/articles/610641-the-impacts-of-assimilating-fengyun-4a-atmospheric-motion-vectors-on-typhoon-forecasts>

1 **The Impacts of Assimilating Fengyun-4A Atmospheric Motion Vectors on Typhoon**
2 **Forecasts**

3 **Keyi Chen¹, Peigen Guan¹**

4 ¹ School of Atmospheric Sciences, Chengdu University of Information Technology, Chengdu,
5 China.

6 Corresponding author: Keyi Chen (ckydlt@aliyun.com)

7 **Key Points:**

- 8 • The data quality of AMVs from the FY-4A are assessed and compared with that from the
9 FY-2G.
- 10 • Assimilating the AMVs from Fengyun satellites can slightly reduce the track errors.
- 11 • Assimilating the AMVs from Fengyun satellites has neutral to positive impacts extending
12 from the upper to the lower level with time.

13 Abstract

14 Atmospheric motion vectors (AMVs), known as cloud track winds, have positive impacts on
15 global numerical weather forecasts (NWP). In this study, AMVs retrieved from Fengyun-2G and
16 Fengyun-4A are compared in their data quality and impacts on the typhoon forecasts in order to
17 investigate the differences between the first and second generation of the geostationary
18 meteorological satellites of China. This report conducted data evaluation and assimilation-
19 forecasting experiments on FY-2G and FY-4A atmospheric motion vector (AMVs), respectively.
20 The results show that the AMVs data of FY-4A are of better quality than those of FY-2G and
21 assimilating the AMVs of FY-2G and FY-4A have a neutral to slightly positive impacts on
22 typhoon forecasts, which is quite encouraging for the operational use in the future.

23 1 Introduction

24 As early as the 1970s, China began to research and develop meteorological satellites. By
25 the end of 2021, China has successfully launched 19 meteorological satellites in total, 7 of which
26 are in orbit, including three polar-orbiting satellites and four geostationary satellites
27 operationally. Fengyun-4A (known as FY-4A) is the first one of China's second-generation
28 geostationary meteorological satellites, which was successfully launched from Xichang Satellite
29 Launch Base on December 11, 2016. On December 17, it was fixed in a geostationary orbit at
30 99.5°E over the equator. Since May 25, 2017, FY-4A drifted to the current position at 105°E for
31 the operational use and its data and products were officially delivered to the users globally from
32 September 25, 2017.

33 Compared with its predecessor (Fengyun-2 series) and other internationally geostationary
34 satellites, Geostationary Interferometric Infrared Sounder (GIIRS) onboard FY-4A is the infrared
35 hyperspectral sounder for the first time in geostationary orbit detecting atmospheric temperature,
36 water vapor, gases, clouds, Earth surface radiations and so on. The advanced Geostationary
37 Radiation Imager (AGRI) with 15 channels provides multi-purpose imagery and wind derivation
38 by tracking clouds and water vapor features. FY-4A is also the first meteorological satellite in
39 the world to achieve comprehensive observation of geostationary orbit imaging and infrared
40 hyperspectral atmospheric vertical detection (Yang et al., 2012).

41 As a new member of Fengyun satellite series, FY-4A has attracted great research interests
42 globally. Zhang et al. (2016) compared FY-4A with Japanese Himawari-8/9 satellites from four
43 aspects of comprehensive detection, instrument observing ability, quantitative application and
44 data service, and found that the two satellites had their own advantages and disadvantages,
45 respectively. Through the study of AGRI/FY-4A, Lu et al. (2017) showed that the observing
46 spectrum settings and spatio-temporal resolutions of the imagers are significantly improved
47 comparing with the first generation of Fengyun satellites. Hansen M C et al. (2000) noticed that
48 the newly added observation channel of AGRI provides a brand new observation support for
49 monitoring atmospheric aerosol, dust/ash, cloud phase and fire point

50 Atmospheric motion vectors (AMVs) is one of the retrieved products of geostationary
51 Fengyun satellite series. It is to retrieve the horizontal wind vectors of the different height levels
52 by tracking the features on the successive multiple satellite images mainly from the infrared and
53 water vapor channels (Xue, 2009). This retrieved product provides data supplement for the lack
54 of wind measuring instruments, especially over the wide open ocean. Previously, meteorologists
55 have studied the AMVs of Fengyun satellite series operationally and scientifically. Mecikalski et

56 al. (2006); Bedka et al. (2009); Mecikalski et al. (2010) evaluated meso-scale atmospheric
 57 motion wind vectors (MAMVs) and proposed that MAMVs could be used to study the
 58 convective mechanism. Height assignment was noted as the dominant factor for the main AMVs
 59 uncertainty suggested by Velden et al. (2009) when comparing the AMVs with the conventional
 60 wind profiles. Aiming to provide detailed uncertainty estimates for the assigned pressure,
 61 Salonen et al. (2015) proposed that best-fit pressure statistics enable reliable information about
 62 the AMV uncertainties in the height assignment, which was an effective method independent on
 63 different data assimilation systems convinced by the Met Office and European Centre for
 64 Medium-Range Weather Forecasts (ECMWF) systems. Liu et al. (2012) used Weather Research
 65 and Forecasting Model Data Assimilation (WRFDA) system to assimilate the AMVs data
 66 retrieved from FY-2C infrared and water vapor channels, and showed that the reasonable
 67 selection of AMVs data added to the numerical weather prediction (NWP) model was beneficial
 68 to supply the meso-scale information not included in the initial fields, as well as improving the
 69 prediction ability of the model. In order to assess the qualities and assimilating impacts of the
 70 AMVs retrieved from the first generation of the Chinese Fengyun geostationary satellite, the
 71 AMVs data of FY-2G and Himawari-8 were evaluated by Liang et al. (2021) in typhoon
 72 forecasts with the conclusions that both AMVs data have showed comparably positive
 73 forecasting impacts even though the AMVs quality of Himawari-8 were overall better.

74 As a type of indirect satellite observation data products, the AMVs can be applied in the
 75 assimilation system in order to provide the important wind information at different height levels,
 76 but few study used the AMVs of FY-4A in the NWP. Therefore, this paper will focus the
 77 assimilating and forecasting impacts of the AMVs of FY-4A. The AMVs data set of Fengyun
 78 satellite series and the NWP model for research and methodology used in this study are
 79 described in the following section. Basic pre-processes before AMVs data assimilation and data
 80 sets assessment will be conducted in the section 3. In Section 4, we selected typhoon In-Fa to
 81 study the assimilation and forecasting impacts of assimilating the AMVs data of FY-2G and FY-
 82 4A on typhoon prediction. Those impacts are verified in typhoon Haishen case in section 5 and
 83 this study concludes in second 6.

84 **2 Data and Methodology**

85 **2.1 WRFDA-3DVAR Assimilation System**

86 The Weather Research and Forecasting Model (WRF) model and Weather Research and
 87 Forecasting Model Data Assimilation (WRFDA) system (Barker et al., 2012) (Version 3.9.1) are
 88 applied for this study by using the 3DVAR component, which can assimilate most of the
 89 conventional observation data and part of the non-conventional observation data (Barker et al.,
 90 2003; Huang, X.Y. et al., 2009; Barker et al., 2012). To obtain a statistically optimal analysis, an
 91 iterative minimization of a prescribed cost function is described by:

$$92 \quad J(\mathbf{x}) = 1/2[(\mathbf{x}-\mathbf{x}^b)^T \mathbf{B}^{-1}(\mathbf{x}-\mathbf{x}^b) + (\mathbf{y}-\mathbf{H}[\mathbf{x}])^T \mathbf{R}^{-1}(\mathbf{y}-\mathbf{H}[\mathbf{x}])] \quad (1)$$

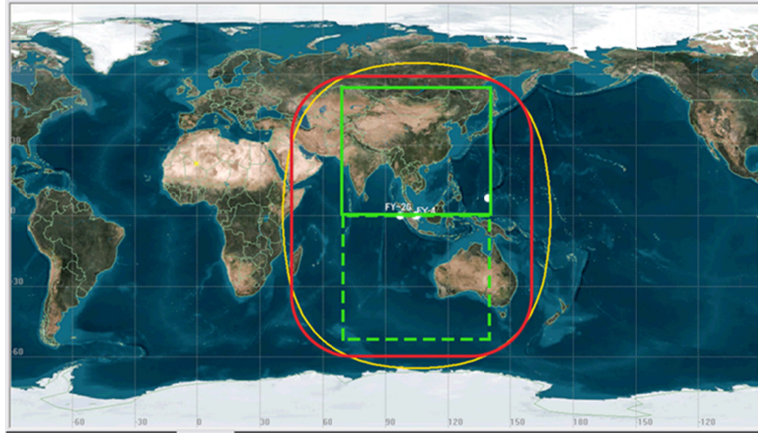
93 where \mathbf{x} represents the atmospheric state vector, \mathbf{x}^b represents the background state, \mathbf{H} represents
 94 the nonlinear observation operator which maps the model variables to the observation space, and
 95 \mathbf{y} represents the observation vector. \mathbf{B} and \mathbf{R} represent the background and observation error
 96 covariance matrices, respectively.

97 2.2 AMVs Data Sets from Fengyun Satellite Series

98 The AMVs data of FY-2G and FY-4A both retrieved from infrared and water vapor
 99 channels provided by The National Satellite Meteorological Center of China (NSMC) are studied
 100 in this report with the aim to compare the assimilating impacts from the first and second
 101 generation of geostationary satellites on typhoon prediction. The AMVs data of FY-2G are
 102 retrieved from images of one infrared channel (10.3-11.3 μm) and one water vapor channel (6.3-
 103 7.6 μm) with a time resolution of 6h(0000 UTC, 0600 UTC, 1200 UTC, 1800UTC) and a
 104 horizontal resolution of 110KM; while the AMVs of FY-4A are retrieved from images of one
 105 infrared channel (10.3-11.3 μm) and two vapor channels (6.9-7.3 μm , 5.8-6.7 μm) with a higher
 106 time resolution of 3h(0000 UTC, 0300 UTC, 0600 UTC, 0900 UTC, 1200 UTC, 1500 UTC,
 107 1800 UTC, 2100 UTC) and the horizontal resolution of 64 km. All retrieved AMVs are divided
 108 into three layers: 100-400 hPa for high-level, 400-700 hPa for middle level, and 700-950 hPa for
 109 lower level and each AMVs data contains latitude, longitude, height, U component, V
 110 component, wind speed, wind direction and quality mark QI with a value range from 0 to 100.
 111 Basically, the larger QI value is, the smaller error of the wind vector will be and the AMVs with
 112 QI larger than 80 are considered to be of good quality. The parameters of the two satellites are
 113 listed in Table 1 and the observing regions of the two satellites are shown in Figure 1. The red
 114 circle and the yellow one indicate the observation area of FY-2G and FY-4A, respectively, and
 115 the green rectangle domain is the overlapped observing area of the two satellites, as well as the
 116 studied regions in this report.

117 Table 1: The channels used for retrieving the AMVs of geostationary satellite FY-2G and
 118 FY-4A.

Satellite	IR Channel (μm)	WV Channel (μm)	Observing Area	Nadir
FY-2G	10.3-11.3	6.3-7.6	55°E-155°E 50°S-50°N	99.5°E
FY-4A	10.3-11.3	6.9-7.3	40°E-170°E 65°S-65°N	105°E
		5.8-6.7		



119

120 Figure 1. The observation area of geostationary satellites FY-2G and FY-4A (the red
 121 circle is for FY-2G; the yellow circle is for FY-4A; the green box is the studied area here; the
 122 solid line is for the northern hemisphere; the dotted line is for the southern hemisphere).

123

2.3 Reanalysis Data

124

125 The final (FNL) operational global analysis data provided by the National Center for
 126 Environmental Prediction (NCEP) are used to initialize the WRF model and update the lateral
 127 boundaries in this study and have a temporal resolution of 6h (0000 UTC, 0600 UTC, 1200
 128 UTC, 1800UTC), a spatial resolution of $0.25^\circ \times 0.25^\circ$ and 26 vertical levels from 1000hPa to
 129 10hPa. This product is from the Global Data Assimilation System (GDAS), which continuously
 130 collects observational data from the Global Telecommunications System (GTS), and other
 131 sources (see more details at <https://rda.ucar.edu/datasets/ds083.2/>). Parameters in the analyses
 132 includes surface pressure, sea level pressure, geopotential height, temperature, sea surface
 133 temperature, soil values, ice cover, relative humidity, u- and v- winds, vertical motion, vorticity
 134 and ozone, except any AMVs information of Fengyun geostationary satellite series
 (https://www.emc.ncep.noaa.gov/gmb/STATS/html/model_changes.html).

135

136 The ERA-5 (1950-present) global reanalysis data from the European Centre for Medium-
 137 Range Weather Forecasts (ECMWF) are used as an independent reference data for verifying the
 138 AMVs data quality of the two Fengyun geostationary satellites. The selected time resolution for
 139 this study is 6h (0000 UTC, 0600 UTC, 1200 UTC, 1800UTC), spatial resolution is $0.25^\circ \times$
 140 0.25° , and vertical levels are from 1000 hPa to 1 hPa as mentioned above
 (<https://confluence.ecmwf.int/pages/viewpage.action?pageId=74764925>).

141

2.4 Typhoon Track and Intensity Data

142

143 The best track data of typhoons provided by the China Meteorological Administration
 144 Tropical Cyclone Database (“CMA best track” is used thereafter for simplicity) with 6-hour
 intervals are used to evaluate the prediction results of the track and intensity of the typhoons.

145

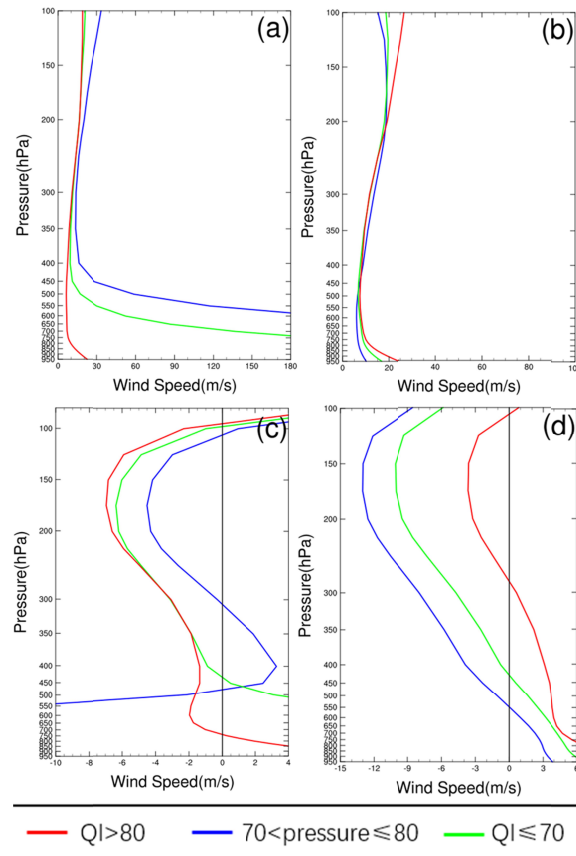
3 The Assessment of the AMVs Data

146

147 Similar to the previous studies (Liang et al., 2021), the AMVs data retrieved from both
 148 Fengyun geostationary satellites have the largest number at the upper level (100-400hPa), as well
 149 as the AMVs with $QI > 80$ from both satellites, regardless of the retrieving channels (the figures
 are not shown). The wind speed bias and root mean square error (RMSE) distribution of the

150 AMVs data from the two satellites (using the AMVs retrieved from the infrared channels as an
 151 example) in the studied green rectangle area of Figure 1 are displayed in Figure 2, referring to
 152 the ERA-5 global reanalysis data. In order to avoid the seasonal differences of the Northern and
 153 Southern Hemisphere, the wind speed bias and RMSE of the two satellites are compared within
 154 the same hemisphere, respectively.

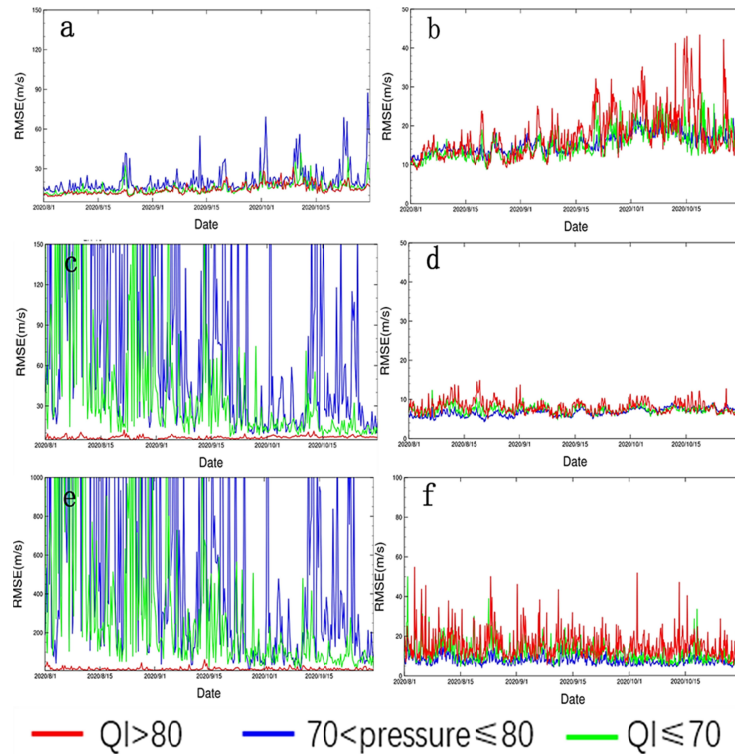
155 Apparently, FY-2G AMVs data with $QI > 80$ have dominantly better quality by showing
 156 smaller and more stable RMSE vertically than those with smaller QI (Figure 2a), while FY-4A
 157 AMVs data with different QI are generally comparable from the lower levels to the upper ones
 158 (Figure 2b). Though the RMSE of FY-4A AMVs data with lower QI values are slightly smaller
 159 than those with $QI > 80$ above 200hPa and below 475hPa, the biases of the former is much
 160 smaller than the latter regarding to the whole atmospheric levels (Figure 2d). Comparatively, the
 161 biases of FY-2G AMVs data with $QI > 80$ are larger with the value range from -7m/s to 4m/s.
 162 Similar results are found for the AMVs data retrieved from the water vapor channels of the two
 163 geostationary satellites and for the studied southern Hemisphere area. This indicates that the
 164 overall quality of the AMVs data from FY-4A as the second generation meteorological satellite
 165 of China is improved than those from the first generation satellite FY-2G.



166

167 Figure 2. The vertical distributions of the RMSE (upper row) and the bias (lower row) of
 168 the full wind speed of the AMVs data retrieved from the infrared channels for the Northern
 169 Hemisphere referring to the ERA5 global reanalysis data. ((a) and (c) are for FY-2G, and (b) and
 170 (d) are for FY-4A. Red line represents the AMVs with QI larger than 80, blue line represents the
 171 AMVs with QI between 70 and 80, green line represents the AMVs with QI smaller than 70.

172 The RMSE time series of the AMVs data retrieved from the infrared channels of the two
 173 satellites at different height levels from August 1 2020 to October 31 2020 are described in
 174 Figure 3. Similarly to the previous results, the RMSE and its variations with time of the AMVs
 175 data from FY-4A at different levels are quite comparable regardless of their QI values.
 176 Compared to those from FY-2G, the RMSE values of FY-4A AMVs data are much smaller with
 177 a smaller time variation. For FY-2G AMVs data, only those with $QI > 80$ show reliable data
 178 quality. This further demonstrates that the AMVs data of FY-4A have better and more reliable
 179 quality than those of the first generation of Fengyun geostationary satellites..

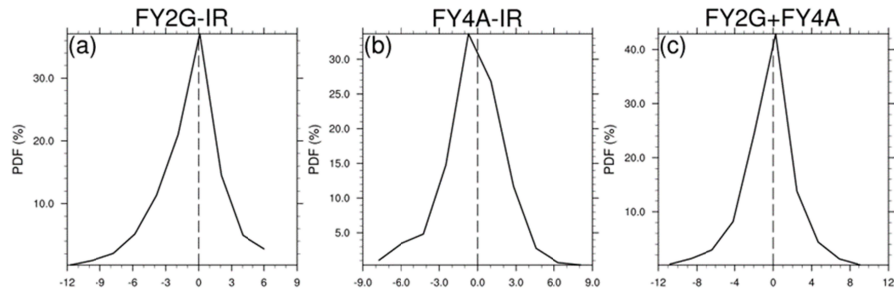


180
 181 Figure 3. The RMSE time series of the AMVs data retrieved from the infrared channels at
 182 different height levels from August 1 2020 to October 31 2020. The red line represents the
 183 AMVs data with QI larger than 80; the blue line represents the AMVs data with QI between 70
 184 and 80; and the green line represents the AMVs data with QI smaller than 70. (a), (c), (e) are for
 185 FY-2G and (b), (d), (f) are for FY-4A. The upper row are for 100 ~400hPa; the middle row are
 186 for 400 ~700hPa; and the lower row are for 700 ~950hPa.

187 Considering the AMVs data characteristics, a series of quality control processes,
 188 including height assignment, quality control, background check, observation error assignment,
 189 channel merging and thinning, are conducted referring to Liang et al.(2021).

190 The WRFDA-3DVAR assimilation system applied in this paper requires that the
 191 assimilated AMVs data are unbiased (Gaussian distribution). Figure 4 shows the Probability
 192 density distribution (PDF) of the first guess departures (O-B) of the AMVs data retrieved from
 193 the infrared channels of FY-2G and FY-4A after quality control processes at 12:00 UTC on July
 194 22 2020 (similar results for water vapor channels, not shown). Undoubtedly, the PDF of FY-4A
 195 is more unbiased with a much narrower normal shape than that of FY-2G and also the first guess

196 departures of the combined AMVs data of the two satellites meet the unbiased requirements of
 197 the 3DVAR method, which insures that the assimilating experiments can be carried out.



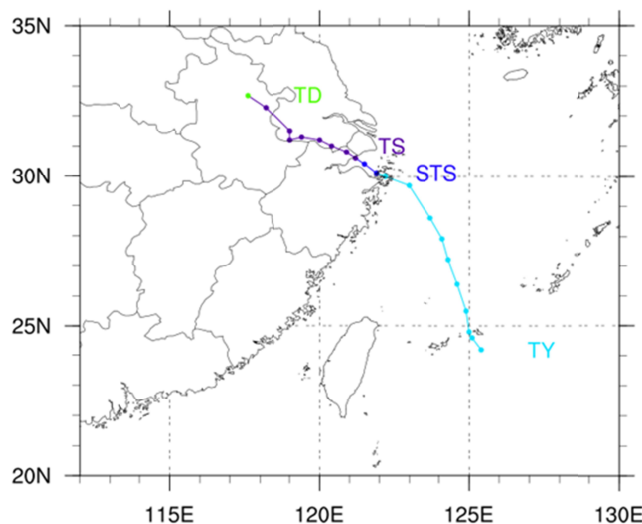
198

199 Figure 4. The Probability density distribution of the first guess departures (O-B) of the
 200 AMVs data retrieved from the infrared channels of FY-2G and FY-4A after quality control
 201 processes at 12:00 UTC on July 22, 2020 (a for FY2G, b for FY4A, and c for the combined
 202 FY2G and FY4A).

203 4 AMVs Data Assimilation Experiments Studies

204 4.1 Overview of Severe Typhoon In-Fa

205 Typhoon In-Fa, the 6th typhoon forming in the Western Pacific Ocean in 2021 had a
 206 predominantly northwestward path (Figure 5), which is selected to study the assimilating and
 207 forecasting impacts of AMVs from the two Fengyun geostationary satellites. At 0200 UTC on
 208 July 18, the Central Meteorological Agency (CMA) upgraded it to a tropical storm based on the
 209 observations and then upgraded it to a strong typhoon at 1100 UTC on July 21. Typhoon In-Fa
 210 made its landfall on the coastal of Zhejiang Province at 1200 UTC on July 25, and made landfall
 211 again on the coastal area of Pinghu county, Zhejiang Province at 0900 UTC on July 26. In-Fa
 212 weakened in Anhui province on July 28 and then gradually moved northwestward. The main
 213 characteristics of Typhoon “In-Fa” include slow moving speed, long retention time over land,
 214 and large cumulative rainfall. A total of 4.82 million people in Zhejiang, Shanghai and Jiangsu
 215 provinces were affected by Typhoon In-Fa, with a direct economic loss of 13.2 billion RMB.



216

217 Figure 5. The CMA best track of In-Fa from 0000 UTC on July 23, 2021 to 2100 UTC on
 218 July 27, 2021 (interval: 6h; TD: Tropical Depression TS: Tropical Storm; STS: Severe Tropical
 219 Storm; TY: Typhoon).

220 4.2 Experimental settings

221 To compare the assimilating and forecasting impacts of the retrieved AMVs data from
 222 different channels of the two Fengyun geostationary satellites on the forecasts of Severe
 223 Typhoon In-Fa, 9 experiments are set up, including one control experiment and 8 cycling
 224 assimilation experiments with assimilating the AMVs data retrieved from infrared and water
 225 vapor imaging channels of FY-2G and FY-4A, respectively (Table 2). FY2G-IR, FY2G-IR+WV
 226 and FY2G+FY4A are used to illustrate the assimilating experiment settings. FY2G-IR indicates
 227 that the AMVs data retrieved from the infrared images of FY-2G satellite are assimilated in the
 228 cycling experiment, while the AMVs data retrieved from the infrared and water vapor images of
 229 FY-2G are assimilated in FY2G-IR+WV experiment and all the AMVs data from both FY-2G
 230 and FY-4A satellites are assimilated in FY2G+FY4A experiment regardless the retrieved
 231 channels.

232 Table 2: The List of the Assimilating Experiment Settings.

Experiments	ID	Settings
Control experiment	CONT	Without data assimilated
cycling assimilation experiments	FY2G-IR	FY-2G AMVs data from the infrared channel assimilated
	FY2G-WV	FY-2G AMVs data from the water vapor channel assimilated
	FY2G-IR+WV	FY-2G AMVs data from the combined channels assimilated
	FY4A-IR	FY-4A AMVs data from the infrared channel assimilated
	FY4A-WV1	FY-4A AMVs data from the lower water vapor channel assimilated
	FY4A-WV2	FY-4A AMVs data from the higher water vapor channel assimilated

	FY4A-IR+WV	FY-4A AMVs data from the combined channels assimilated
	FY2G+FY4A	FY-2G+FY-4A AMVs data from all the five retrieved channels assimilated

233 The model integration time is from 0000 UTC on July 22 2021, after the tropical storm
 234 was strengthened to Typhoon In-Fa, to 0000 UTC on July 28 2021, after its landfall and
 235 weakening, for the all nine experiments, with the model configuration including 300×300 grids
 236 centering at (28°N, 120°E), the horizontal resolution of 15km, the time step 60 seconds, the 40
 237 eta layers in the vertical direction and the model top at 10hPa.

238 The cycling analysis-forecast experiments starting from 1200 UTC on July 22 2021 with
 239 the AMVs data assimilated every 12h are carried out with different settings. Except the first 12
 240 hours for the spin-up time, nine DA cycles are performed in total with a 6h assimilating window.
 241 The National Meteorological Center method (NMC; Parrish & Derber, 1992) is applied to assign
 242 the background error covariance by calculating the forecast differences between the 24-h and 12-
 243 h forecasts. The background for the first analysis is the forecast initiated from the FNL analysis
 244 at 1200UTC on July 22 2021 and the backgrounds for the following cycles are the 12h model
 245 forecasts initialized from the previous analyses of last cycles. In addition, table 3 lists the
 246 physical parameterization schemes adopted in all nine assimilating experiments.

247 Table 3: The List of the Parameterization Schemes Used for All the Nine Experiments for
 248 Typhoon In-Fa.

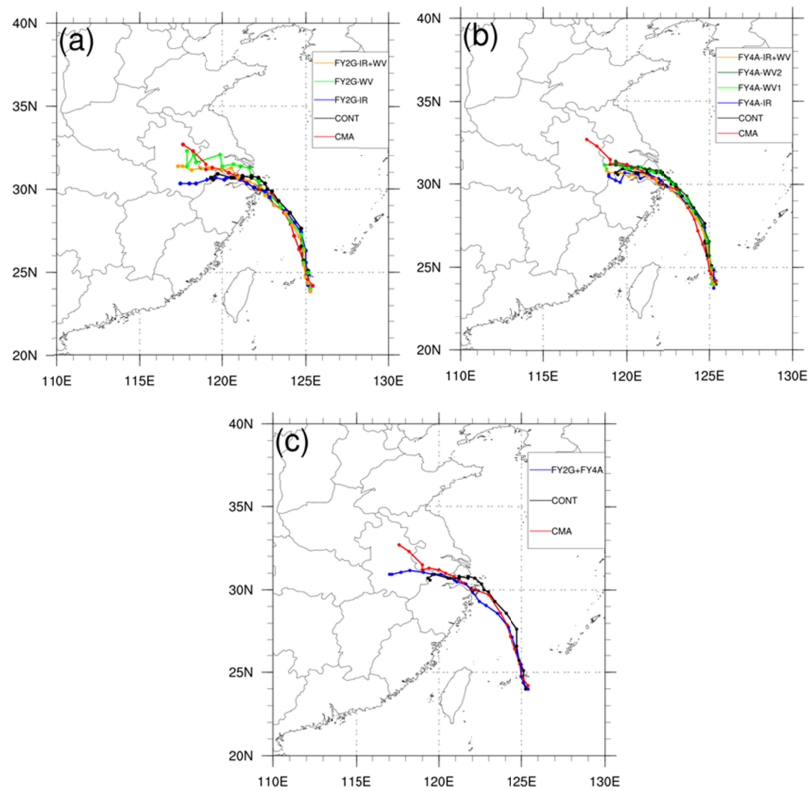
parameterization schemes	settings
Microphysics scheme	Lin (Lin et al, 1983)
Cumulus convection scheme	Tiedtke (Tiedtke, M. et al., 1989)
radiation scheme	RRTMG /RRTMG (Mlawer et al., 1997)
Planetary boundary layer scheme	MYJ (Janjic et al., 1994)
Land-surface scheme	Noah (Niu et al., 2011)

249 4.3 Forecasting Impacts on Typhoon In-Fa

250 4.3.1 Impacts on the Typhoon Track and Intensity Forecasts

251 Figure 6 displays the forecasting tracks of Typhoon In-Fa in all nine experiments verified
 252 by the CMA best track data since In-Fa made its landfall in East China. Basically, the results of
 253 the eight cycling assimilation experiments are slightly better compared to the control run by
 254 showing tracks closer to the CMA data (Figure 6a and 6b). Before the landfall, those eight

255 forecasting tracks in the assimilation runs are quite comparable and track differences are more
 256 clear after the landfall which might be due to the impacts of the surfaces. Undoubtedly, the
 257 forecasting typhoon paths in FY2G-IR+WV and FY4A-IR+WV perform the best in their group
 258 and experiment FY2G+FY4A shows the best typhoon track overall with the most AMVs
 259 assimilated for the best fitting in this study. Compare 6a and 6b, the forecasted typhoon moving
 260 speeds in FY4A assimilating experiments (Figure 6b) are slower than those in FY2G
 261 assimilating experiments (Figure 6a) after the typhoon makes landfall. From the perspective of
 262 typhoon track forecasts, assimilating the AMVs of FY-2G and FY-4A can significantly improve
 263 the deviation of typhoon track simulation than the control experiment, effectively improve the
 264 typhoon path and make the forecast path closer to the real situation of the typhoon movement,
 265 but the slower moving speeds in the assimilating experiments which contain FY4A AMVs need
 266 to be further investigated to know the reason.



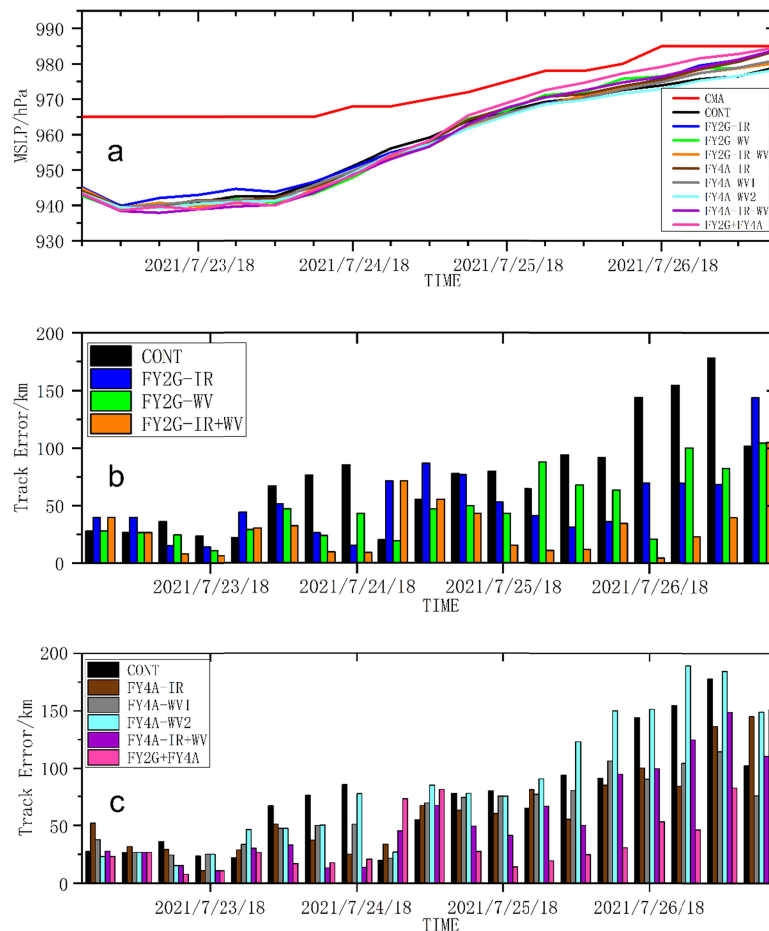
267

268 Figure 6. The evolution of track (a-c) referring to the CMA best track of Typhoon In-Fa
 269 from 0000 UTC on July 23 2021 to 0000 UTC on July 28 2021 (interval:6h; red: CMA best
 270 track; black: CONT; for a-c). For (a), yellow line represents experiment FY2G-IR+WV; green
 271 line represents experiment FY2G-WV; blue line represents experiment FY2G-IR. For (b), yellow
 272 line represents experiment FY4A-IR+WV; light blue line represents experiment FY4A-WV2;
 273 green line represents experiment FY4A-WV1; blue line represents experiment FY4A-IR. For (c),
 274 blue line represents experiment FY2G+FY4A.

275 At present, forecasts of typhoon intensity are still a difficult problem for each operational
 276 center. As shown in Figure 7a, the control and the assimilation experiments have similar
 277 intensity variation trends of typhoon In-Fa by overestimating the typhoon intensity at the early
 278 stage and approaching to the best track provided by the China Meteorological Agency (CMA)

279 since 1800 UTC on July 24 2021. From the perspective of typhoon intensity forecasts,
 280 assimilating the AMVs of FY-2G and FY-4A have neutral impacts.

281 In order to accurately compare the differences of typhoon track forecasts between all
 282 experiments, Figure 7b and 7c shows the track error (unit: km) of each experiment. Assimilating
 283 the AMVs from the merged channels (i.e. FY2G-IR+WV, FY4A-IR+WV, FY2G+FY4A) does
 284 indicate some benefits by showing generally smaller track errors, which also grow more slowly,
 285 than CONT, especially from 1800 UTC on July 25. Interestingly, 1800 UTC on July 25 is like a
 286 pitch point, before which the variations of the track errors in the eight cycled assimilating
 287 experiments are quite comparable regardless of the satellites and channels. While afterwards, the
 288 experiments with FY2G AMVs data assimilated achieve better results than those with FY4A
 289 AMVs, which may be as a results of that the forecasting typhoon moving speeds in FY4A
 290 assimilating experiments are slower than those in FY2G runs after the simulated landfall of
 291 typhoon.



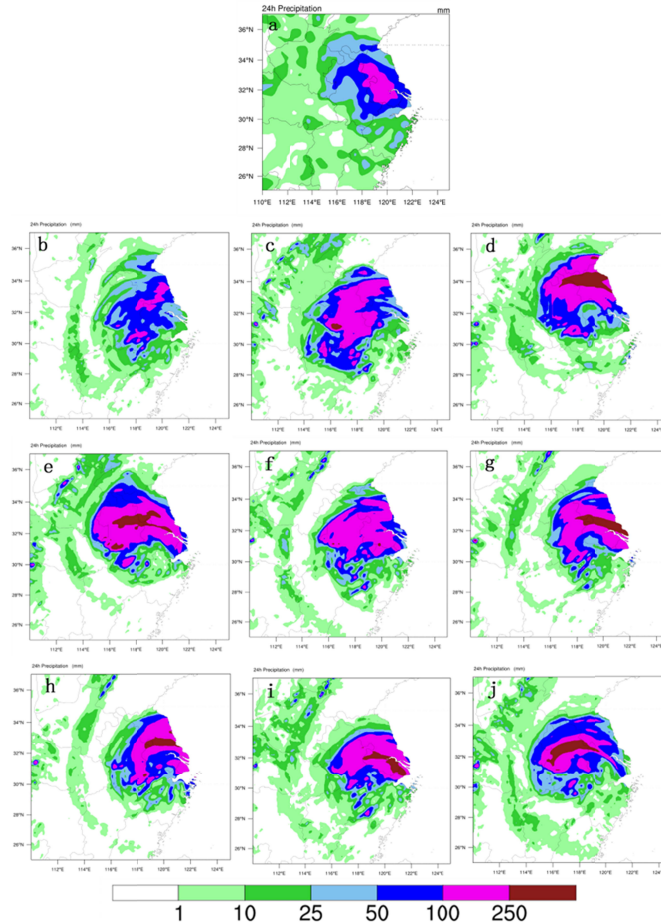
292

293 Figure 7. The evolution of intensity (MSLP, unit: hPa) and track errors (b-c unit: km)
 294 referring to the CMA best track data of Typhoon In-Fa from 0000 UTC on July 23 2021 to 0000
 295 UTC on July 28 2021, the time interval is 6h. (black line and bar: CONT; blue line and bar:
 296 FY2G-IR; green line and bar: FY2G-WV; orange line and bar: FY2G-IR+WV; brown line and
 297 bar: FY4A-IR; grey line and bar: FY4A-WV1; light blue line and bar: FY4A-WV2; purple line

298 and bar: FY4A-IR+WV; pink line and bar: FY2G+FY4A; for a-c). For (a), red line represents the
 299 CMA best track.

300 4.3.2 Impacts on the Typhoon Precipitation Forecasts

301 As indicated by the observations of the hourly intensive automatic rainfall stations of the
 302 CMA (China Meteorological Administration) (Figure 8a), heavy precipitation over 100 mm
 303 mainly occurred in the east coast of China with the precipitation region located in Jiangsu and
 304 Anhui provinces. However, the precipitation in CONT is much underestimated than the
 305 observations (Figure 8b). While, all assimilating experiments overestimate the rainfall amount,
 306 which might be related to the overestimation of the typhoon intensity in each run, except that the
 307 experiment FY2G+FY4A corrects this kind of precipitation overestimation to some extent with
 308 the closest typhoon intensity to the CMA data. Comparing among the results with assimilating
 309 the AMVs from different channels, the experiments with those from water vapor channels
 310 (Figure 8d 8g 8h) are more likely to cause excessive precipitation forecasts than those from
 311 infrared channels (Figure 8c and 8f), which may be due to that the AMVs of the water vapor
 312 channel lack of the wind field information in the middle and lower levels of the atmosphere.

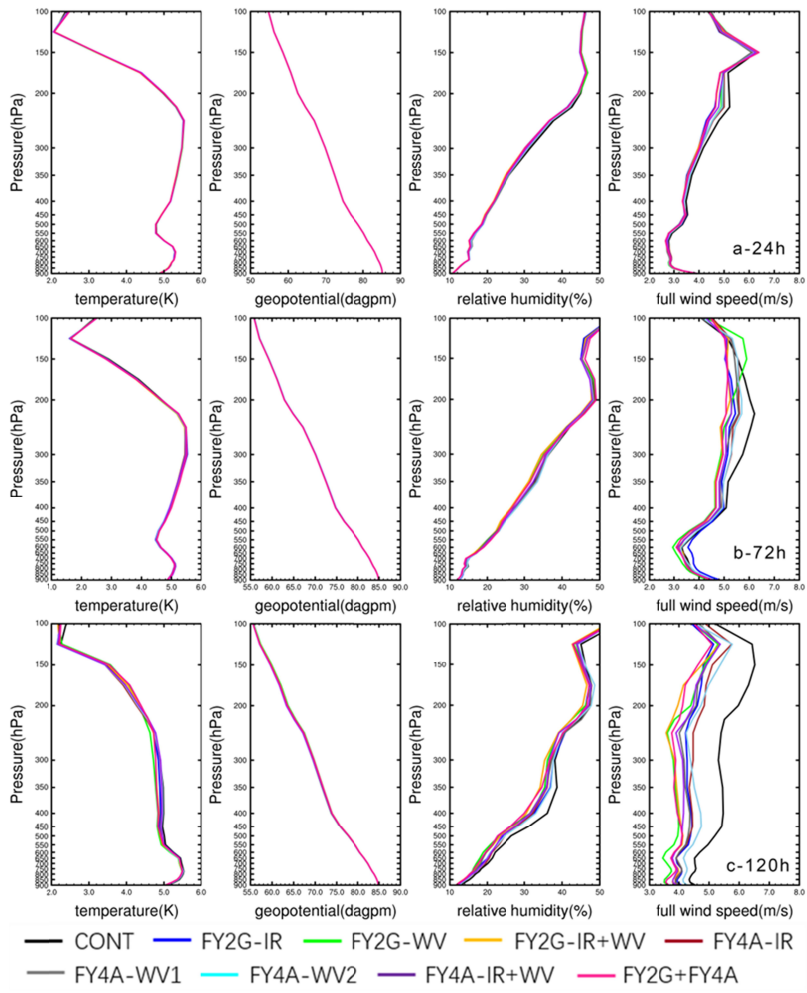


313

314 Figure 8. The 24-h accumulated precipitation (unit: mm) over land from 0000 UTC on
 315 July 27, 2021 to 0000 UTC on July 28, 2021 from CMA observations of the hourly intensive
 316 automatic rainfall stations (a), CONT (b), FY2G-IR (c), FY2G-WV (d), FY2G-(IR+WV) (e),
 317 FY4A-IR (f), FY4A-WV1 (g), FY4A-WV2 (h), FY4A-(IR+WV) (i) and FY2G+FY4A (j)
 318 experiments.

319 4.3.3 Forecasting Impacts on the Physical Variables Fields

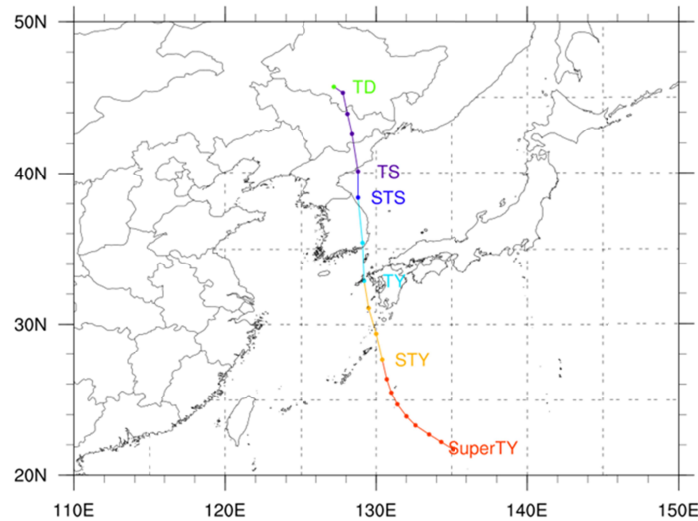
320 The vertical profiles of the root mean square error (RMSE) at 24-h, 72-h and 120-h
 321 forecasts of temperature, geopotential height, relative humidity and full wind speed started from
 322 0000 UTC on July 23 2021 referring to the ECMWF ERA5 reanalysis data in the control run and
 323 eight assimilating experiments are calculated in order to quantitatively evaluate the assimilating
 324 and forecasting impacts on the longer-period forecasts and the values smaller than those of
 325 CONT indicate the positive impacts (Figure 9). Basically, the impacts on geopotential height and
 326 temperature are neutral from the lower level to the upper level with the time evolution. For the
 327 relative humidity field, slightly positive impacts are shown at 72-h forecast above 350hPa, which
 328 propagate down to near surfaces, and more evident improvements are displayed at 120-h
 329 forecasts for the entire vertical atmospheric levels. More dominantly positive impacts on the full
 330 wind speed occur above 450hPa at 24-h forecast, and extend to all levels at 72-h forecast, then
 331 become much more dramatic at 120-h forecast. Apparently, assimilating the AMVs data from the
 332 two Fengyun geostationary satellites in all experiments improves the most of the full wind speed
 333 forecasts than the forecasts of other physical variable fields vertically and the impacts extend
 334 from the upper level down to the lower level with the forecasting time evolution, for that there
 335 are the largest AMVs data amounts at the upper level. FY2G+FY4A experiment shows generally
 336 better positive impacts over all than others, which may be in the result of that the most
 337 observations assimilated provide a better fitting for the analysis.



339 Figure 9. Vertical profiles of the 24-h (a), 72-h (b), and 120-h (c) forecast RMSEs
 340 referring to the ECMWF ERA5 reanalysis data of temperature (unit: K), geopotential height
 341 (unit: dagpm), relative humidity (unit: %) and the full wind speed (unit: m s^{-1}) fields started
 342 from 0000 UTC on July 23 2021 from the control experiment (CONT) (black), FY2G – IR
 343 (blue), FY2G – WV (green), FY2G – IR + WV (yellow), FY4A – IR (dark purple), FY4A – WV1
 344 (gray), FY4A-WV2(light blue), FY4A_IR+WV(purple) and FY2G+FY4A(purple red).

345 5 Verification of the Assimilation Impacts on Typhoon Forecasts

346 The results above demonstrate that the main impacts of assimilating the AMVs data from
 347 the two Fengyun geostationary satellites are neutral to slightly positive and basically the more
 348 AMVs data assimilated, the more improvements are shown. Aiming to verify this, more
 349 assimilating experiments are conducted. A series experiments for typhoon Haishen which is the
 350 10th typhoon occurring in the Western Pacific Ocean in 2020 are studied here as a verification
 351 case. Haishen had a predominantly northward path (Figure 10). 9 experiments are also set up
 352 (Table 2) as mentioned above and the physical parameterization schemes adopted in all nine
 353 experiments are listed in Table 4.



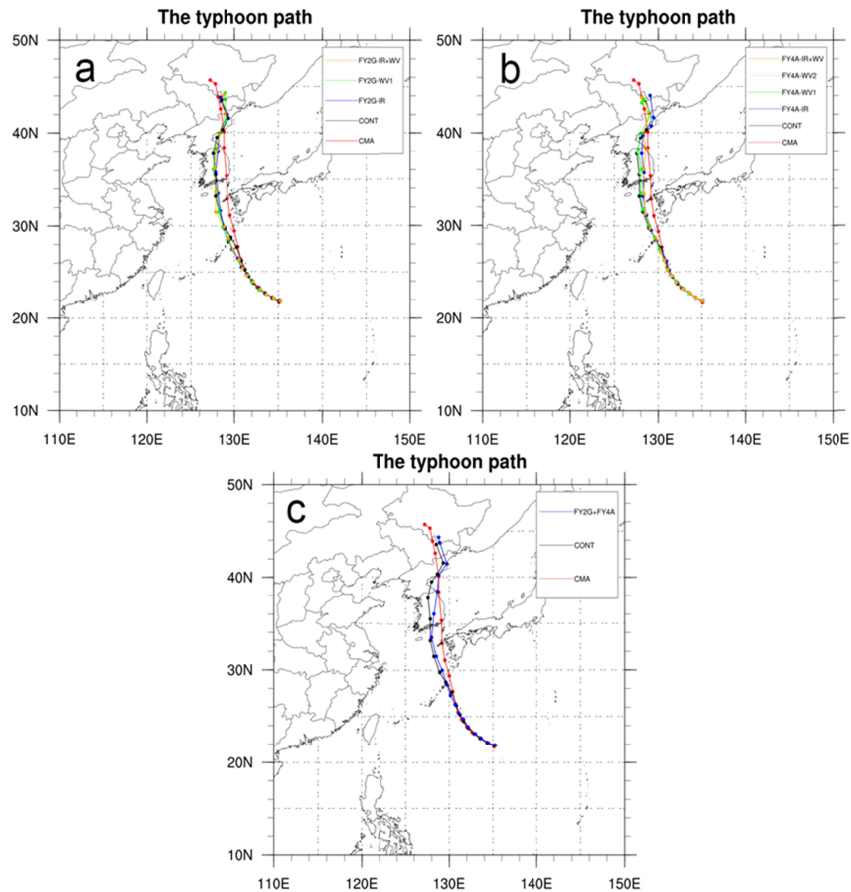
354
 355 Figure 10. The CMA best track of Haishen from 0000 UTC on September 4, 2020 to
 356 1200 UTC on September 8, 2020 (interval: 6h; TD: Tropical Depression; TS: Tropical Storm;
 357 STS: Severe Tropical Storm; TY: Typhoon STY: Severe Typhoon; SuperTY: Super Typhoon).

358 Table 4: The List of the Parameterization Schemes Used for all the Nine Experiments for
 359 Typhoon Haishen.

The Physical Parameterization Schemes		Configurations
Microphysics Scheme		Lin (Lin et al., 1983)
Planetary Boundary Layer Scheme		Yonsei University scheme (Hong et al., 2006)
Radiation Scheme	Long-wave	RRTM scheme (Mlawer et al., 1997)
	Short-wave	Dudhia scheme (Dudhia, 1989)

Cumulus Convection Scheme	Kain-Fritsch scheme (Kain, 2004)
Land-Surface Scheme	MM5 similarity (Fairall et.al., 2003)

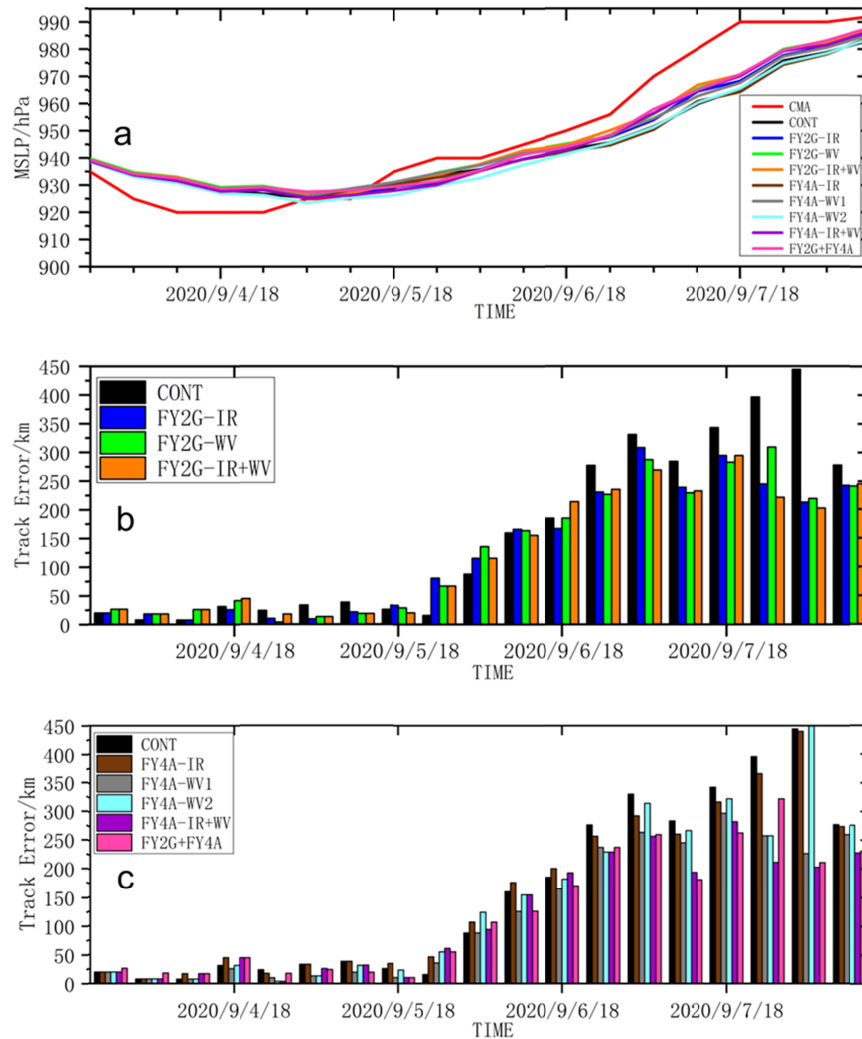
360 Compared to the best track, the typhoon tracks in CONT and all assimilating experiments
 361 are almost the same with the best track for the first 48h (before 1200 UTC on September 5, 2020)
 362 before they start to deviate (Figure 11). While, the typhoon track forecasts of all assimilation
 363 experiments start to approach to the best track than that in CONT since 0000 UTC September 7
 364 2020, especially for the experiments FY4A-IR+WV and FY2G+FY4A. Basically, more neutral
 365 to slightly positive impacts of forecasting and assimilation are still displayed with time varying,
 366 even with such a number of the AMVs data assimilated in each experiment.



367
 368 Figure 11. The evolution of track (a-c) referring to the CMA best track of Typhoon
 369 Haishen from 0000 UTC on September 4, 2020 to 1200 UTC on September 8, 2020 (interval:6h;
 370 red: CMA best track; black: CONT; for a-c). For (a), yellow line represents experiment FY2G-
 371 IR+WV; green line represents experiment FY2G-WV; blue line represents experiment FY2G-IR.
 372 For (b), yellow line represents experiment FY4A-IR+WV; light blue line represents experiment
 373 FY4A-WV2; green line represents experiment FY4A-WV1; blue line represents experiment
 374 FY4A-IR. For (c), blue line represents experiment FY2G+FY4A.

375 As shown in Figure 12a, compared with the intensity evolution of Typhoon Haishen
 376 provided by the CMA Tropical Cyclone Data Center., the control and assimilation experiments
 377 have similar intensity variation trends, but the occurrence time of the lowest MSLP is later in all

378 assimilation experiments than that in the best track data. Generally, the results of all cycling
 379 experiments are comparable, but slightly better forecasts are shown by the experiments with
 380 assimilating FY-4A AMVs data, and the best track forecasts are obtained from Experiment
 381 FY4A-IR+WV (Figure 12c), which indicates the advantages of channel merging. It also verifies
 382 that FY-4A, as China's second-generation meteorological satellite, has improved the data quality
 383 compared with FY-2G.

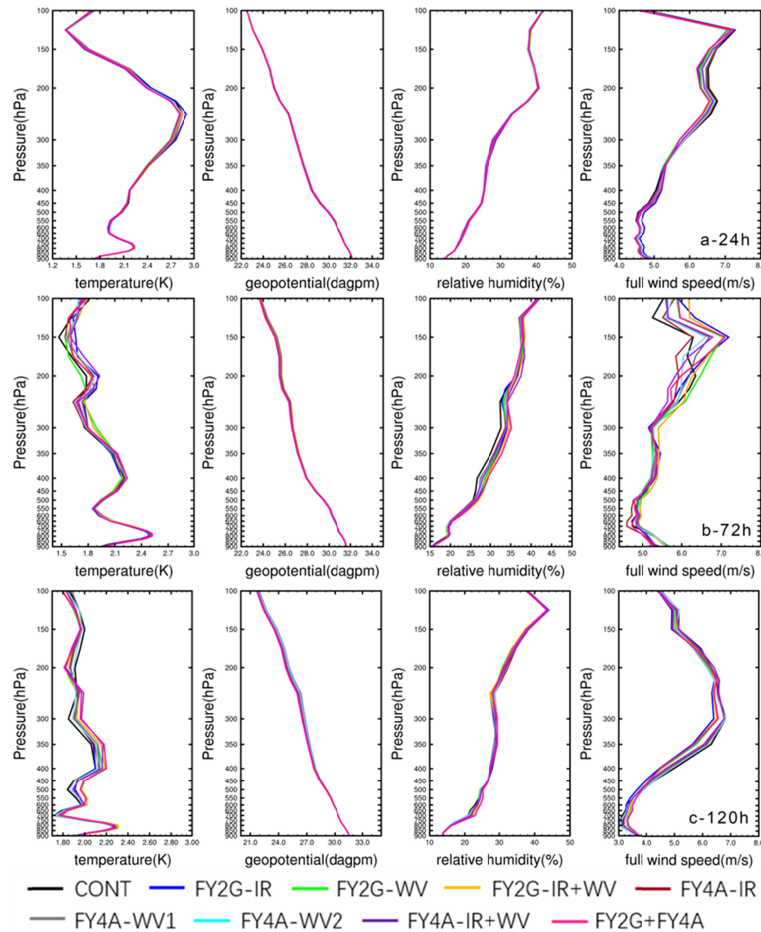


384

385 Figure 12. The evolution of intensity (a MSLP, unit: hPa) and track errors (b-c unit: km)
 386 referring to the CMA best track of Typhoon Haishen from 0000 UTC on September 4, 2020 to
 387 1200 UTC on September 8, 2020 (black: CONT; blue: FY2G-IR; green: FY2G-WV; orange:
 388 FY2G-IR+WV; brown: FY4A-IR; grey: FY4A-WV1; light blue: FY4A-WV2; purple: FY4A-
 389 IR+WV; pink: FY2G+FY4A; for a-c). For (a), red line represents CMA best track.

390 For the forecast impacts on the physical variable fields, comparable improvements are
 391 still achieved in all assimilation experiments for the full wind speed. Slightly positive impacts on
 392 the full wind speed occur above 300hPa at 24-h forecast, and extend to 600hPa at 120-h forecast.
 393 The longer the forecast time is, the more positive impacts are shown (Figure 13). Similar to the
 394 previous results, assimilating the AMVs data from the two Fengyun geostationary satellites has

395 neutral to slightly positive impacts vertically on the full wind speed more evidently than other
 396 physical variables fields and the impacts extend from the upper level down to the lower level,
 397 since there are the largest AMVs data at the upper level. Though the main impacts are generally
 398 neutral, FY2G+FY4A experiment still shows a bit better positive impacts than others.



399

400 Figure 13. Vertical profiles of the 24-h (a), 72-h (b), and 120-h (c) forecast RMSEs
 401 versus the ECMWF ERA5 reanalysis of temperature (unit: K), geopotential height (unit: dagpm),
 402 relative humidity (unit: %) and the full wind speed (unit: m s^{-1}) fields from the control
 403 experiment (CONT) (black), FY2G – IR (blue), FY2G – WV (green), FY2G – IR + WV (yellow),
 404 FY4A – IR (dark purple), FY4A– WV1 (gray), FY4A-WV2(light blue), FY4A_IR+WV(purple)
 405 and FY2G+FY4A(purple red).

406 6 Conclusion and Discussion

407 In order to evaluate the quality, assimilating and forecasting impacts of the AMVs data
 408 retrieved from the Chinese second generation geostationary meteorological satellite FY-4A in
 409 the typhoon forecasts within a limited domain by applying the WRFDA system with the 3D-
 410 VAR component, the AMVs from the first generation geostationary meteorological satellite FY-
 411 2G are used as an assessing reference in the overlapping observing region of the two. This study
 412 indicate that the retrieved AMVs from the infrared and water vapor channels of the two Fengyun
 413 satellites are mainly located at the middle and upper levels (100hPa to 700hPa) and only a few at
 414 the low level (700hPa to 950hPa), which are consistent with previous AMVs studies. For full

415 wind speeds, FY-4A AMVs show generally better data quality with smaller and stable RMSEs
416 and biases than those of FY-2G.

417 Typhoon In-Fa is selected and eight cycling assimilation experiments and one control run
418 are carried out to study the impacts of assimilation and forecasting by assimilating the two
419 AMVs data on the typhoon forecasts, which are exhibited to be basically comparable for the
420 forecasted typhoon tracks. Convincingly, assimilating the AMVs of both FY-2G and FY-4A can
421 slightly reduce the track errors compared with CONT. However, there are no significant positive
422 impacts for the typhoon intensity prediction and only neutral impacts are founded, which
423 indicates that the typhoon intensity prediction is still a hard question for the NWP.

424 It is noticed that the experiments with the AMVs retrieved from water vapor channels are
425 more likely to cause excessive rainfall amount in the typhoon precipitation prediction over land
426 than those from infrared channels. Moreover, the physical variables field forecasts illustrate that
427 assimilating the AMVs data from Fengyun geostationary satellites has neutral to positive impacts
428 on the full wind speed more evidently than other physical variables fields vertically and the
429 impacts extend from the upper level down to the lower level with time evolution since there are
430 the largest number of the AMVs data at the upper level. The verification experiment of typhoon
431 Haishen confirms the conclusions above by showing the similar assimilating and forecasting
432 results.

433 As the new generation of Chinese geostationary satellite in meteorology, FY-4A has not
434 only upgraded its instruments, but also provide data with better quality than its predecessor FY-
435 2G. The results in the studies here are quite encouraging for the NWP application. Though the
436 forecasting and assimilating impacts are basically neutral to slightly positive, the retrieved
437 AMVs data are still worthy of being further investigated in order to be applied operationally.
438 Lately, more FY-4 satellite series are about to be launched subsequently and more AMVs data
439 can be retrieved from multiple channels and applied not only for the NWP, but also for various
440 research purposes.

441 **Acknowledgments**

442 The authors appreciate the National Natural Science Funds of China to support this research
443 through Grant No. 41875039 and also thank the National Key Scientific and Technological
444 Infrastructure project “Earth System Science Numerical Simulator Facility” (EarthLab) for its
445 support (Grant No.:2022-EL-PT-00052). The FY2G and FY4A AMVs data were obtained freely
446 from (<http://satellite.nsmc.org.cn/portalsite/Data/DataView.aspx/>). The ECMWF analysis and the
447 NCEP data can be downloaded from
448 (<https://cds.climate.copernicus.eu/cdsapp#!/dataset/reanalysis-era5-pressure-levels>) and
449 (<https://rda.ucar.edu/datasets/ds083.3/>), respectively. The precipitation observations can be
450 obtained from (<http://data.cma.cn/data/cdcindex/cid/f0fb4b55508804ca.html/>).

451 **References**

452 Barker D M, Huang W, Guo Y R, et al. A three-dimensional variational (3DVAR) data
453 assimilation system for use with MM5[J]. NCAR Tech Note, 2003, 68.
454 <https://doi.org/10.5065/D6CF9N1J>

- 455 Barker D, Huang X Y, Liu Z, et al. The weather research and forecasting model's community
456 variational/ensemble data assimilation system: WRFDA[J]. Bulletin of the American
457 Meteorological Society, 2012, 93(6): 831-843. <https://doi.org/10.1175/BAMS-D-11-00167.1>
- 458 Bedka, K. M., Velden, C. S., Petersen, R. A., Feltz, W. F., & Mecikalski, J. R. (2009).
459 Comparisons of satellite-derived atmospheric motion vectors, rawinsondes, and NOAA wind
460 profiler observations. *Journal of Applied Meteorology and Climatology*, 48(8), 1542– 1561.
461 <https://doi.org/10.1175/2009JAMC1867.1>
- 462 Dudhia, J. (1989). Numerical study of convection observed during the winter monsoon
463 experiment using a mesoscale two-dimensional model. *Journal of the Atmospheric Sciences*,
464 46(20), 3077–3107. [https://doi.org/10.1175/1520-0469\(1989\)046<3077:nsocod>2.0.co;2](https://doi.org/10.1175/1520-0469(1989)046<3077:nsocod>2.0.co;2)
- 465 Fairall, C. W., Bradley, E. F., Hare, J. E., Grachev, A. A., & Edson, J. B. (2003). Bulk
466 parameterization of air-sea fluxes: Updates and verification for the COARE algorithm. *Journal of*
467 *Climate*, 16(4), 571–591. [https://doi.org/10.1175/1520-0442\(2003\)016<0571:BPOASF>2.0.CO;2](https://doi.org/10.1175/1520-0442(2003)016<0571:BPOASF>2.0.CO;2)
- 469 Hansen M C, Reed B. A comparison of the IGBP DIS Cover and University of Maryland 1
470 km global land cover products [J] . *Int J Remote Sens*, 2000, 21(6):1365-1373. 21
471 <https://doi.org/10.1080/014311600210218>
- 472 Hong, S. Y., Noh, Y., & Dudhia, J. (2006). A new vertical diffusion package with an explicit
473 treatment of entrainment processes. *Monthly Weather Review*, 134(9), 2318–2341.
474 <https://doi.org/10.1175/mwr3199.1>
- 475 Huang, X.Y., Q. Xiao, D.M. Barker, X. Zhang, J. Michalakes, W. Huang, T. Henderson, J. Bray,
476 Y. Chen, Z. Ma, J. Dudhia, Y. Guo, X. Zhang, D.J. Won, H.C. Lin, and Y.H. Kuo, 2009: Four-
477 Dimensional Variational Data Assimilation for WRF: Formulation and Preliminary Results.
478 *Mon. Wea. Rev.*, 137, 299–314. <https://doi.org/10.1175/2008MWR2577.1>
- 479 Janjic, Zavisla I., 1994: The Step–Mountain Eta Coordinate Model: Further developments of the
480 convection, viscous sublayer, and turbulence closure schemes. *Mon. Wea. Rev.*, 122, 927–945.
481 [https://doi.org/10.1175/1520-0493\(1994\)122%3c0927:TSMECM%3e2.0.CO;2](https://doi.org/10.1175/1520-0493(1994)122%3c0927:TSMECM%3e2.0.CO;2)
- 482 Kain, J. S. (2004). The Kain-Fritsch convective parameterization: An update. *Journal of Applied*
483 *Meteorology*, 43, 170–181. [https://doi.org/10.1175/1520-0450\(2004\)043<0170:tkcpau>2.0.co;2](https://doi.org/10.1175/1520-0450(2004)043<0170:tkcpau>2.0.co;2)
- 484 Liang, J., Chen, K., & Xian, Z. (2021). Assessment of FY - 2G Atmospheric Motion Vector
485 Data and Assimilating Impacts on Typhoon Forecasts. *Earth and Space Science*, 8(6),
486 e2020EA001628. <https://doi.org/10.1029/2020EA001628>
- 487 Li, Y., K. Y. Chen, and Z. P. Xian, 2021: Evaluation of All-Sky assimilation of FY-3C/MWHS-2
488 on Mei-Yu precipitation forecasts over the Yangtze-Huaihe River Basin. *Adv. Atmos. Sci.*,
489 <https://doi.org/10.1007/s00376-021-0401-y>.
- 490 Liu Rui, Zhai Guoqing, Wang Zhanggui, et al. Experimental study on the influence of FY-2C
491 Cloud Track Wind Data Assimilation on typhoon forecast [J]. *Chinese Journal of Atmospheric*
492 *Sciences*, 2012, 36(2): 350-360. Doi: CNKI:SUN:DQXK.0.2012-02-012(in Chinese).
- 493 Lin, Y., Farley, R., & Orville, H. (1983). Bulk parameterization of the snow field in a cloud
494 model. *Journal of Climate and Applied Meteorology*, 22, 1065–1092.
495 [https://doi.org/10.1175/1520-0450\(1983\)022<1065:BPOTSF>2.0.CO;2](https://doi.org/10.1175/1520-0450(1983)022<1065:BPOTSF>2.0.CO;2)

- 496 Lu F, Zhang X H, Chen B Y, et al., 2017.FY-4 geostationary meteorological satellite
497 imaging characteristics and its application prospects[J].J Mar Meteor, 37 (2) : 1-12.doi:
498 10.19513/j.cnki.issn2096-3599.2017.02.001. (in Chinese) .
- 499 Mecikalski, J. R., & Bedka, K. M. (2006). Forecasting convective initiation by monitoring the
500 evolution of moving cumulus in daytime GOES imagery. *Monthly Weather Review*, 134(134),
501 49– 78. <https://doi.org/10.1175/MWR3062.1>
- 502 Mecikalski, J. R., Bedka, K. M., Paech, S. J., & Litten, L. A. (2008). A statistical evaluation of
503 GOES cloud-top properties for nowcasting convective initiation. *Monthly Weather Review*,
504 136(12), 4899– 4914. <https://doi.org/10.1175/2008MWR2352.1>
- 505 Mlawer, E. J., Taubman, S. J., Brown, P. D., Iacono, M. J., & Clough, S. A. (1997). Radiative
506 transfer for inhomogeneous atmospheres:RRTM, a validated correlated-k model for the
507 longwave. *Journal of Geophysical Research*, 102(D14), 16663–16682.
508 <https://doi.org/10.1029/97JD00237>
- 509 Niu, Guo–Yue, Zong–Liang Yang, Kenneth E. Mitchell, Fei Chen, Michael B. Ek, Michael
510 Barlage, Anil Kumar, Kevin Manning, Dev Niyogi, Enrique Rosero, Mukul Tewari, Youlong
511 Xia, 2011: The community Noah land surface model with multiparameterization options (Noah–
512 MP): 1. Model description and evaluation with local–scale measurements. *J. Geophys. Res.*, 116,
513 D12109. <https://doi.org/10.1029/2010JD015139>
- 514 Peng Zhang, Qiang Guo, Boyang Chen, Xuan Feng. Comparative analysis of Chinese Fy-4
515 meteorological satellite and Japanese Himawari-8/9 satellite [J]. *Progress in meteorological*
516 *science and technology*,2016,6(01):72-75(in Chinese).
- 517 Salonen K, Cotton J, Bormann N, et al. Characterizing AMV Height-Assignment Error by
518 Comparing Best-Fit Pressure Statistics from the Met Office and ECMWF Data Assimilation
519 Systems[J]. *J.appl.meteor.climatol*, 2014, 54(42):5647-5653. [https://doi.org/10.1175/JAMC-D-](https://doi.org/10.1175/JAMC-D-14-0025.1)
520 [14-0025.1](https://doi.org/10.1175/JAMC-D-14-0025.1)
- 521 Tiedtke, M., 1989: A comprehensive mass flux scheme for cumulus parameterization in large–
522 scale models. *Mon. Wea. Rev.*, 117, 1779–1800.[https://doi.org/10.1175/1520-](https://doi.org/10.1175/1520-0493(1989)117<1779:ACMFSF>2.0.CO;2)
523 [0493\(1989\)117<1779:ACMFSF>2.0.CO;2](https://doi.org/10.1175/1520-0493(1989)117<1779:ACMFSF>2.0.CO;2)
- 524 Velden C S, Bedka K M. Identifying the Uncertainty in Determining Satellite-Derived
525 Atmospheric Motion Vector Height Attribution[J]. *Journal of Applied Meteorology &*
526 *Climatology*, 2009, 48(3):450-463. <https://doi.org/10.1175/2008JAMC1957.1>
- 527 Xue, J. (2009). The scientific problems and prospects of meteorological satellite data
528 assimilation. *Acta Meteorologica Sinica*, 67(6), 903– 911 (in Chinese).
529 <https://doi.org/10.3321/j.issn:0577-6619.2009.06.001>
- 530 Yang Jun, et al. *Meteorological satellites and their applications*. Beijing: China Meteorological
531 Press, 2012(in Chinese)

532 **Figures Captions:**

533 Figure 1. The observation area of geostationary satellites FY-2G and FY-4A (the red circle is for
534 FY-2G; the yellow circle is for FY-4A; the green box is the studied area here; the solid line is for
535 the northern hemisphere; the dotted line is for the southern hemisphere).

536 Figure 2. The vertical distributions of the RMSE (upper row) and the bias (lower row) of the full
537 wind speed of the AMVs data retrieved from the infrared channels for the Northern Hemisphere
538 referring to the ERA5 global reanalysis data. ((a) and (c) are for FY-2G, and (b) and (d) are for
539 FY-4A. Red line represents the AMVs with QI larger than 80, blue line represents the AMVs
540 with QI between 70 and 80, green line represents the AMVs with QI smaller than 70.

541 Figure 3. The RMSE time series of the AMVs data retrieved from the infrared channels at
542 different height levels from August 1 2020 to October 31 2020. The red line represents the
543 AMVs data with QI larger than 80; the blue line represents the AMVs data with QI between 70
544 and 80; and the green line represents the AMVs data with QI smaller than 70. (a), (c), (e) are for
545 FY-2G and (b), (d), (f) are for FY-4A. The upper row are for 100 ~400hPa; the middle row are
546 for 400 ~700hPa; and the lower row are for 700 ~950hPa.

547 Figure 4. The Probability density distribution of the first guess departures (O-B) of the AMVs
548 data retrieved from the infrared channels of FY-2G and FY-4A after quality control processes at
549 12:00 UTC on July 22, 2020 (a for FY2G, b for FY4A, and c for the combined FY2G and
550 FY4A).

551 Figure 5. The CMA best track of In-Fa from 0000 UTC on July 23, 2021 to 2100 UTC on July
552 27, 2021 (interval: 6h; TD: Tropical Depression TS: Tropical Storm; STS: Severe Tropical
553 Storm; TY: Typhoon).

554 Figure 6. The evolution of track (a-c) referring to the CMA best track of Typhoon In-Fa from
555 0000 UTC on July 23 2021 to 0000 UTC on July 28 2021 (interval:6h; red: CMA best track;
556 black: CONT; for a-c). For (a), yellow line represents experiment FY2G-IR+WV; green line
557 represents experiment FY2G-WV; blue line represents experiment FY2G-IR. For (b), yellow line
558 represents experiment FY4A-IR+WV; light blue line represents experiment FY4A-WV2; green
559 line represents experiment FY4A-WV1; blue line represents experiment FY4A-IR. For (c), blue
560 line represents experiment FY2G+FY4A.

561 Figure 7. The evolution of intensity (MSLP, unit: hPa) and track errors (b-c unit: km) referring
562 to the CMA best track data of Typhoon In-Fa from 0000 UTC on July 23 2021 to 0000 UTC on
563 July 28 2021, the time interval is 6h. (black line and bar: CONT; blue line and bar: FY2G-IR;
564 green line and bar: FY2G-WV; orange line and bar: FY2G-IR+WV; brown line and bar: FY4A-
565 IR; grey line and bar: FY4A-WV1; light blue line and bar: FY4A-WV2; purple line and bar:
566 FY4A-IR+WV; pink line and bar: FY2G+FY4A; for a-c). For (a), red line represents the CMA
567 best track.

568 Figure 8. The 24-h accumulated precipitation (unit: mm) over land from 0000 UTC on July 27,
569 2021 to 0000 UTC on July 28, 2021 from CMA observations of the hourly intensive automatic
570 rainfall stations (a), CONT (b), FY2G-IR (c), FY2G-WV (d), FY2G-(IR+WV) (e), FY4A-IR
571 (f),FY4A-WV1 (g),FY4A-WV2(h),FY4A-(IR+WV)(i) and FY2G+FY4A(j) experiments.

572 Figure 9. Vertical profiles of the 24-h (a), 72-h (b), and 120-h (c) forecast RMSEs referring to
573 the ECMWF ERA5 reanalysis data of temperature (unit: K), geopotential height (unit: dagpm),

574 relative humidity (unit: %) and the full wind speed (unit: m s^{-1}) fields started from 0000 UTC
575 on July 23 2021 from the control experiment (CONT) (black), FY2G – IR (blue), FY2G – WV
576 (green), FY2G – IR + WV (yellow), FY4A – IR (dark purple), FY4A – WV1 (gray), FY4A-
577 WV2(light blue), FY4A_IR+WV(purple) and FY2G+FY4A(purple red).

578 Figure 10. The CMA best track of Haishen from 0000 UTC on September 4, 2020 to 1200 UTC
579 on September 8, 2020 (interval: 6h; TD: Tropical Depression; TS: Tropical Storm; STS: Severe
580 Tropical Storm; TY: Typhoon STY: Severe Typhoon; SuperTY: Super Typhoon).

581 Figure 11. The evolution of track (a-c) referring to the CMA best track of Typhoon Haishen from
582 0000 UTC on September 4, 2020 to 1200 UTC on September 8, 2020 (interval:6h; red: CMA
583 best track; black: CONT; for a-c). For (a), yellow line represents experiment FY2G-IR+WV;
584 green line represents experiment FY2G-WV; blue line represents experiment FY2G-IR. For (b),
585 yellow line represents experiment FY4A-IR+WV; light blue line represents experiment FY4A-
586 WV2; green line represents experiment FY4A-WV1; blue line represents experiment FY4A-IR.
587 For (c), blue line represents experiment FY2G+FY4A.

588 Figure 12. The evolution of intensity (a MSLP, unit: hPa) and track errors (b-c unit: km)
589 referring to the CMA best track of Typhoon Haishen from 0000 UTC on September 4, 2020 to
590 1200 UTC on September 8, 2020 (black: CONT; blue: FY2G-IR; green: FY2G-WV; orange:
591 FY2G-IR+WV; brown: FY4A-IR; grey: FY4A-WV1; light blue: FY4A-WV2; purple: FY4A-
592 IR+WV; pink: FY2G+FY4A; for a-c). For (a), red line represents CMA best track.

593 Figure 13. Vertical profiles of the 24-h (a), 72-h (b), and 120-h (c) forecast RMSEs versus the
594 ECMWF ERA5 reanalysis of temperature (unit: K), geopotential height (unit: dagpm), relative
595 humidity (unit: %) and the full wind speed (unit: m s^{-1}) fields from the control experiment
596 (CONT) (black), FY2G – IR (blue), FY2G – WV (green), FY2G – IR + WV (yellow), FY4A –
597 IR (dark purple), FY4A – WV1 (gray), FY4A-WV2(light blue), FY4A_IR+WV(purple) and
598 FY2G+FY4A(purple red).

599

600

601

602

603

604

605

606

607

608

609

610

611

612 Table 1: The channels used for retrieving the AMVs of geostationary satellite FY-2G and
 613 FY-4A.

Satellite	IR Channel (μm)	WV Channel (μm)	Observing Area	Nadir
FY-2G	10.3-11.3	6.3-7.6	55°E-155°E 50°S-50°N	99.5°E
FY-4A	10.3-11.3	6.9-7.3	40°E-170°E 65°S-65°N	105°E
		5.8-6.7		

614

615

616

617

618

619

620

621

622

623

624 Table 2: The List of the Assimilating Experiment Settings

Experiments	ID	Settings
Control experiment	CONT	Without data assimilated
	FY2G-IR	FY-2G AMVs data from the infrared channel assimilated

cycling assimilation experiments	FY2G-WV	FY-2G AMVs data from the water vapor channel assimilated
	FY2G-IR+WV	FY-2G AMVs data from the combined channels assimilated
	FY4A-IR	FY-4A AMVs data from the infrared channel assimilated
	FY4A-WV1	FY-4A AMVs data from the lower water vapor channel assimilated
	FY4A-WV2	FY-4A AMVs data from the higher water vapor channel assimilated
	FY4A-IR+WV	FY-4A AMVs data from the combined channels assimilated
	FY2G+FY4A	FY-2G+FY-4A AMVs data from all the five retrieved channels assimilated

625

626

627

628

629

630 Table 3: The List of the Parameterization Schemes Used for All the Nine Experiments for
631 Typhoon In-Fa.

parameterization schemes	settings
Microphysics scheme	Lin (Lin et al, 1983)
Cumulus convection scheme	Tiedtke (Tiedtke, M. et al., 1989)
radiation scheme	RRTMG /RRTMG (Mlawer et al., 1997)

Planetary boundary layer scheme	MYJ (Janjic et al., 1994)
Land-surface scheme	Noah (Niu et al., 2011)

632

633

634

635

636

637

638

639

640

641 Table 4: The List of the Parameterization Schemes Used for all the Nine Experiments for
642 Typhoon Haishen.

The Physical Parameterization Schemes		Configurations
Microphysics Scheme		Lin (Lin et al., 1983)
Planetary Boundary Layer Scheme		Yonsei University scheme (Hong et al., 2006)
Radiation Scheme	Long-wave	RRTM scheme (Mlawer et al., 1997)
	Short-wave	Dudhia scheme (Dudhia, 1989)
Cumulus Convection Scheme		Kain-Fritsch scheme (Kain, 2004)
Land-Surface Scheme		MM5 similarity (Fairall et.al., 2003)

643